Hybrid DC-Bus Capacitor Discharge Strategy Using Internal Windings and External Bleeder for Surface-mounted PMSM based EV Powertrains in Emergency

Chao Gong, *Student Member, IEEE*, Yihua Hu, *Senior Member, IEEE*, Wenzhen Li, Jinqiu Gao, Jinglin Liu, *Member, IEEE*, Huiqing Wen, *Senior Member, IEEE*, Jiankang Yang

***Abstract*— When electric vehicles (EVs) encounter an emergency, the voltage of the DC-bus capacitor in the surface-mounted permanent magnet synchronous motor (SPMSM) based powertrain requires to be reduced as fast as possible. In order to eliminate the disadvantages and synthesize the advantages of the traditional machine winding-based and external bleeder-based discharge techniques, this paper proposes a hybrid discharge strategy which can achieve five-second discharge in minimum sacrifice of the bleeder size and weight for any EV drives. For the purpose of evaluating the size reduction of the new method, the individual bleeder-based scheme is modelled and analyzed at first. Then, the combined discharge method is developed, which contains two sequential procedures: bleeding resistor (BR) design and discharge control algorithm design. The BR design process has to be implemented under the extreme condition. But concerning that the emergency might occur at the moment when the machine operates below the maximum speed, three different discharge modes including full-power, partial-power and bleeder-based discharge modes are developed. The proposed discharge techniques are verified by experiments which are conducted on a three-phase SPMSM drive system used for EVs.**

***Index Terms*— Permanent magnet synchronous machine, machine windings, DC-bus capacitor, bleeding resistor, voltage discharge.**

Manuscript received August 25, 2019; revised November 27, 2019 and January 9, 2020; accepted February 06, 2020. This work was supported by Newton Advanced Fellowship, the UK (NAF\R1\191153) (Corresponding author: Yihua Hu).

C. Gong and Y. Hu are with the Department of Electronic Engineering, University of York, Heslington, York, YO10 5DD, U.K. (E-mail: 1452101806@qq.com, yihua.hu@york.ac.uk).

W. Li, J. Gao, J. Liu and J. Yang are with the School of Automation, Northwestern Polytechnical University, and Shaanxi Key Laboratory of Small & Special Electrical Machine and Drive Technology, Xi'an 710129, China (e-mail: 729211047@qq.com, 18829234832@163.com, jinglinl@nwpu.edu.cn, 837951123@qq.com).

H. Wen is with the Department of Electrical and Electronic Engineering, Xi'an Jiaotong-Liverpool University, Suzhou 215123, China. (E-mail: Huiqing.Wen@xjtlu.edu.cn).

I. INTRODUCTION

DUE to the intrinsic advantages of high efficiency, high power density, compact structure and broad speed regulation range, permanent magnet synchronous machines (PMSM) have been widely adopted in electric vehicles (EV) [1]-[10]. The topology of a typical PMSM-based EV propulsion system is shown in Fig.1, which can be separated into the electrical and mechanical parts. In the electrical system, the battery packs are used to store and supply power. The DC-DC boost converter can lift the voltage level, transferring the low voltage into the high one. The voltage source inverter (VSI) converts the direct current (DC) power into the alternating current (AC) power, driving the machine to operate. Moreover, a breaker connecting the battery packs and the converter is adopted for protection, and a bus capacitor in parallel with the inverter needs to be installed for high-frequency power surge absorption. In terms of the mechanical part, a gear box that is linked with the PMSM exerts the function of clutch, differential and speed governor. As to the propulsion system, once an emergency (car crash) occurs, the protection mode will be triggered immediately. Meanwhile, the breaker will be tripped immediately to isolate the battery from the other components, and the axle is disconnected from the traction motor by the gear box and the PMSM just rotates with no load [11], [12]. However, in this case, the residual energy stored in the power electronics will maintain the DC-bus capacitor voltage at the high position, posing potential risks to

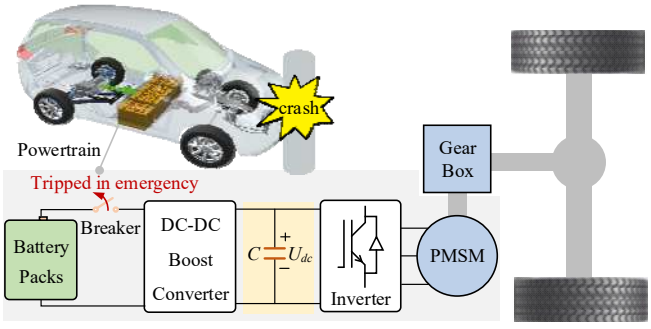

Fig. 1. Topology of typical EV PMSM propulsion system.

both the passengers and the rescuers [13]. In order to avoid electrical shock risks, the EV requires the capacitor voltage to drop to the safe level (60 V) fast (5 s is the best and 60 s is the worst) according to the United Nation Vehicle Regulation ECE R94 [14].

Traditionally, referring to the applications of regenerative braking in [15]-[18], a dynamic braking circuit composed of a switch and a bleeding resistor (BR) is paralleled to the bus capacitor to dissipate the residual energy and discharge the capacitor voltage ("external-circuit discharge"). Whereas, by contrast with the regenerative braking cases, the power and current levels of the braking resistor should be high while the resistance is supposed to be small to satisfy the requirement of quickest discharge. As a result, the size and weight of the bleeding circuit are huge, sacrificing the compactness and cost of the drive system greatly. Practically, the power-downgraded resistors are usually adopted, which cannot reach the highest dissipation velocity.

In addition to the external bleeder-based discharge strategy, several up-to-date studies have presented brand-new machine winding-based discharge approaches which only take advantage of the machine winding resistance to dissipate those residual energy in the form of heating [11-13], [19-21]. This kind of bleeding method can be categorized as "non-external-circuit discharge", which is also a hot topic in the converter applications [22], [23]. As for the winding-based discharge method for EV powertrains, the occasional emergency will not immediately trigger a protection mode and turn off the transistors in the power inverter. Instead, the specially designed d, q-axis currents are injected into the machine to motivate it to operate normally. In [12] and [19], the q-axis current is controlled to stabilize at zero while the d-axis reference current is set as a large constant. But [13], [20] and [21] illustrate that this kind of strategy will lose efficacy when the initial machine speed is higher than the threshold value ω_{th} at which the line-to line back electromotive force (EMF) is 60 V, otherwise the bus capacitor will get recharged (voltage rises) even when its voltage approaches zero. In order to solve this problem, the improved discharge methods based on both voltage and current regulation is proposed in these researches. In addition, literature [11] points out that the performance of the winding-based discharge algorithms is highly related to the system parameters (eg., rotor inertia and system safe current), and although the optimized algorithms in [20] and [21] have been successfully applied to some certain drives whose parameters are suitable for discharge, it is not universally suitable for the other systems with harsh conditions. On this ground a particular bus capacitor discharge technique is developed for the PMSM drives with large inertia and small system safe current. However, there still exist two crucial problems for this strategy. Firstly, the impact of the winding resistance on the discharge characteristics is not considered. In practice, the vehicle propulsion motor is usually designed with small resistance for the sake of loss reduction [24]-[26]. Once the resistance is smaller, the discharge method will no longer be effective to meet the fast discharge requirement, representing that the discharge capacity is limited. Secondly, the voltage discharge velocity (VDV) does not reach the maximum value because the segmented q-axis current that generates the electromagnetic braking torque should be small in case of voltage surges. Now, these defects have hindered the extensive use of this discharge approach.

This paper proposes a hybrid DC-bus capacitor discharge strategy relying on both the machine windings and external bleeder circuits to achieve the five-second discharge in minimum sacrifice of the bleeder size and weight for any EV drives. Compared to the methods in the papers [11-13] and [15-23], the novel approach synthesizes the advantages and overcome the disadvantages of those two traditional strategies. Specifically, the bleeder-based strategy is less dependent of the system parameters and endowed with enormous dissipation capacity so that it can be employed in any EV drives technically, while it is unwanted considering the factors of size, weight and cost; Although the winding-based scheme is much more compact, the system parameters have a strong impact on the discharge performance. Considering these aspects, for a fixed PMSM drive, the machine windings can be adopted as the auxiliary plant for the external bleeder circuits so as to reduce its size, achieving a relatively lightweight and cost-effective discharge technique suited to any EV drives. In this paper, the defects of the external bleeder-based strategy are firstly discussed, figuring out the necessity of the assistant bleeding method. Then, systematic design procedures are developed to achieve the composite discharge approach, which include two main sequential parts: external BR calculation and discharge algorithm design. It should be mentioned that the segmented q-axis current injection approach in [11] is not needed any more, and by using a constant braking current, the VDV can be maximized.

The rest of the paper is organized as follows: Section II initially analyzes the mechanism and sacrifice of the traditional individual external bleeder-based discharge method. Section III describes the proposed energy dissipation strategy and assesses the improvement compared with the traditional method. In Section IV, the discharge performance characteristics of the combined methods are compared according to the experimental results. Section V is the conclusion part.

II. Mechanism and Sacrifice of Bleeder-based Discharge Method

This part will analyze the mechanism of the bleeder-based discharge method. Then, the current level, resistance, size and weight of the BR is theoretically discussed, illustrating that a combined discharge strategy is highly desired. Considering that the discharge request would occur not only in the vehicle driving conditions but also in the parking situations, comprehensive analysis will be carried out concerning both aspects. During discharge, only the motor, inverter, capacitor and bleeder circuits in the EV powertrain are likely to operate. For the sake of simplicity, the equivalent discharge circuits are extracted as shown in Fig.2, where U_a, U_b and U_c are the phase back EMF, L_s and R_s are the motor inductance and resistance, respectively. s and R_b represent the control switch and BR.

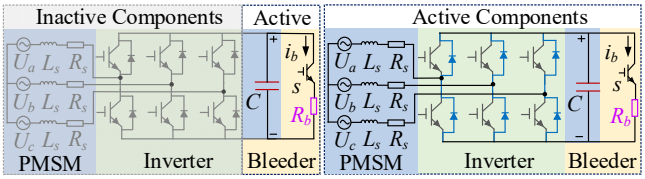

Fig. 2. Equivalent circuits and mechanism of discharge. (a) Standstill cases. (b) Running cases.

A. Mechanism and BR for Standstill Cases

When an initiative discharge is requested at the machine speed of zero, no residual energy is stored in the motor and only the DC-bus capacitor voltage requires to be diminished. Therefore, the PMSM and inverter are inactive while the capacitor and the bleeder circuits are activated. In this case, the capacitor and the bleeder constitute a simple resistance-capacitance (RC) net, so the real-time capacitor voltage U_{dc} during discharge is represented as:

$$U_{dc} = U_{dc0} \cdot e^{-\frac{t}{R_b C}} \tag{1}$$

where U_{dc0} is the initial bus voltage which equals the output of the DC-DC boost converter. C is the capacitance of the bus capacitor. Assuming that the required discharge period and the safe DC-bus voltage are denoted as t_r and U_{safe}, respectively, the required BR can be derived as:

$$R_b \le -\frac{t_r}{C \cdot \ln(\frac{U_{safe}}{U_{dc0}})} \tag{2}$$

When designing a wound-braking-resistor, apart from its resistance, the current-carrying capacity is another crucial parameter that determines the wire size (diameter and length). During the discharge process, the total energy Q_b that needs to be dissipated is:

$$Q_b = \frac{1}{2} C({U_{dc0}}^2 - {U_{safe}}^2) \tag{3}$$

Hence, the root-mean-square (RMS) discharge current i_{bRMS} is:

$$i_{bRMS} = \sqrt{\frac{Q_b}{R_b t_r}} \tag{4}$$

B. Mechanism and BR for Running Cases

If an emergency happens when the vehicle runs on the road, the kinetic energy of the PMSM rotor as well as the energy stored in the bus capacitor should be expended by the BR. In the process of energy consumption, the machine works as a generator, inducing a continuously decreasing back EMF that is related the machine speed. As for the inverter, the emergency triggers the inherent protection mode with "shut-down" control signals applied to all of the transistors. Whereas, the six free-wheeling diodes cannot be sealed off, constituting an uncontrolled rectifier (UR). The back EMF of the machine will be rectified by the UR, charging the capacitor and generating the bleeding current i_b that passes through the BR.

In order to reduce the analytical complexity, an appropriate assumption that the effects of the machine inductance and the capacitor capacitance can be ignored since they are small [27].

TABLE I
PMSM DRIVE SYSTEM PARAMETERS

Parameter	Value	Unit
stator winding resistance R_s	0.15	Ω
number of pole pairs p	3	-
d, q-axis inductance L_d, L_q	0.8	mH
moment of inertia J	0.24	kg·m^2
permanent magnet flux linkage Ψ_f	0.18	Wb
DC-bus voltage U_{dc0}	312	V
safe short-time working current I_{max}	100	A
rated/maximum speed ω_{rated}	345	rad/s
threshold speed ω_{th}	65	rad/s
voltage constant C'_e	2.88	-
required discharge time t_r	5	s
DC-bus capacitor C	560	μF

On this ground the magnitude of the braking q-axis current i_q in the machine equals the bleeding current i_b (active current) and the d-axis current is 0, namely,

$$i_q = -i_b = -\frac{U_{dc}}{R_b} \tag{5}$$

Moreover, according to [28], the bus capacitor voltage can be approximated as:

$$U_{dc} = \sqrt{3} C'_e \Psi_f \omega_m - 2 i_b R_s \tag{6}$$

where C'_e is the voltage constant. Ψ_f is the permanent magnet flux linkage. ω_m is the angular speed. Then, On the basis of the motor model in paper [29], the braking torque T_e of a surface-mounted PMSM (SPMSM) is described as follows:

$$T_e = 1.5 p \Psi_f i_q \approx -1.5 p \Psi_f i_b \tag{7}$$

And the real-time machine speed can be expressed as:

$$\omega_m = \omega_{m0} + \int_0^t \frac{T_e}{J} \mathrm{d}t \tag{8}$$

where ω_{m0} is the initial rotating speed. J is the rotor inertia. Substitute (5), (7) and (8) into (6), U_{dc} can be rewritten as:

$$U_{dc} = \frac{\sqrt{3} J R_b C'_e \Psi_f \omega_{m0} - 1.5\sqrt{3} C'_e p {\Psi_f}^2 \int_0^t U_{dc} \mathrm{d}t}{J(R_b + 2R_s)} \tag{9}$$

Take the derivative of (9), and the voltage descending rate (VDR) can be expressed as:

$$\frac{\mathrm{d}U_{dc}}{\mathrm{d}t} = -\frac{1.5\sqrt{3} C'_e p {\Psi_f}^2}{J(R_b + 2R_s)} U_{dc}(t) \tag{10}$$

Since that U_{dc} experiences a downward trend, according to (10), the voltage VDR will decline continuously as well. Therefore, within t_r, it can be derived that:

$$\int_0^{t_r} U_{dc} \mathrm{d}t \ge (1 + \frac{0.75\sqrt{3} C'_e p {\Psi_f}^2 t_r}{J(R_b + 2R_s)}) t_r U_{safe} \tag{11}$$

Based on (11), the resistance of the BR is supposed to meet the following criteria:

$$R_b \le -\frac{1}{2J(U_{safe} - a)} (4JR_s U_{safe} - 2aJR_s + bU_{safe} t_r - \sqrt{4aJR_s(aJR_s + bU_{safe} t_r) - b^2 U_{safe} {t_r}^2 (U_{safe} - 2a)}) \tag{12}$$

where $a = \sqrt{3} C'_e \Psi_f \omega_{m0}$ and $b = 1.5\sqrt{3} C'_e p {\Psi_f}^2$.

In comparison with the zero-speed cases, the expended energy includes not only the electrical part stored in the capacitor but also the kinetic energy in the machine rotor.

TABLE II
PROPERTIES OF BLEEDING RESISTOR

Resistor properties	Standstill	Running	Unit
resistance R_b	≤ 5415	≤ 7.33	Ω
current level i_{bRMS}	0.03	19.2	A
minimum diameter d_b	0.022	4.5	mm
required length l_b	4.2	237.8	m
calculated mass m_b	$0.014 \cdot 10^{-3}$	33.6	kg

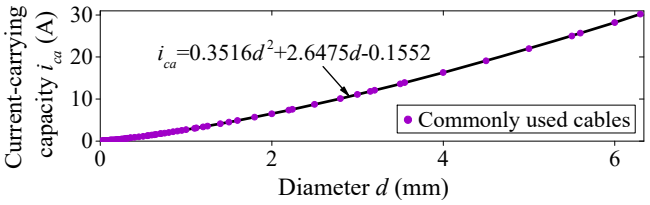

Fig. 3. Relationship between conductor diameter and current-carrying capacity.

$$Q_b = \underbrace{\frac{1}{2}J(\omega_{m0}^{\ 2} - \omega_{th}^{\ 2})}_{Q_1\text{: Kinetic energy}} + \underbrace{\frac{1}{2}C(U_{dc0}^{\ 2} - U_{safe}^{\ 2})}_{Q_2\text{: Electrical energy}} \tag{13}$$

Then, the RMS discharge current is:

$$i_{bRMS} = \sqrt{\frac{Q_b}{(R_b + R_s)t_r}} \tag{14}$$

C. Evaluation of Size and Weight Sacrifice

In order to implement an intuitive discussion on the properties of the BR, a PMSM drive system for EV with parameters in Table I is studied. Currently, one of the most common materials used for making precise braking resistor is the alloy of copper (Cu) and nickel (Ni) [30]. Taking CuNi44 (ISOTAN@) whose resistivity is ρ_r=49·10^{-8} Ω·m and density is ρ_m=8900 kg/m^3 as an example, the minimum wire diameter is selected based on the relationship between the wire diameter d and the current-carrying capacity i_{ca} (as in Fig.3).

$$i_{ca} = 0.3516d^2 + 2.6475d - 0.1552 \tag{15}$$

Table II shows the properties of the BR (just the conductor part) when the required discharge time is 5 s. Firstly, it can be seen that the parameters designed for the running mode (initial speed should be set as the maximum value) are suitable for the standstill situations. Then, to satisfy the fastest discharge requirement, although the required resistance is only 7.33 Ω, the diameter d_b of the conductor is 4.5 mm and the length l_b is 237.8 m, weighing around 33.6 kg. However, such an enormous resistor is unwelcome because it increases the vehicle weight greatly, so in practice, the lower power-level resistors are usually used, but the discharge time will exceed 5 s.

Overall, the EVs are placing a high demand on the novel discharge strategies characterized by rapid discharge but small size and weight.

III. PROPOSED HYBRID DISCHARGE TECHNIQUE

Fig.4 illustrates the block diagram of the proposed hybrid discharge strategy. Compared to Fig.2, the novel bleeding system is composed of not only the motor, diodes and external

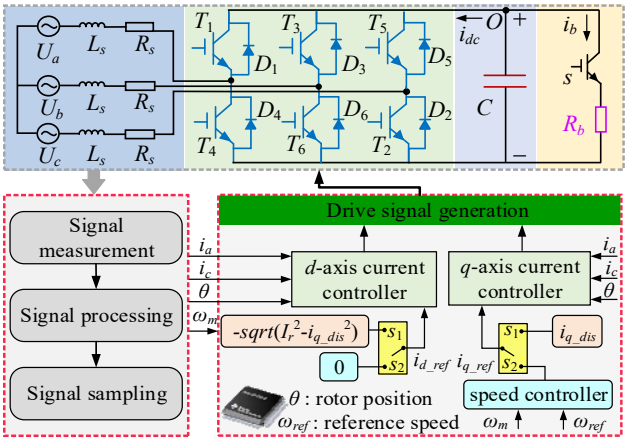

Fig. 4. Block diagram of the proposed hybrid discharge method.

bleeder circuits but also the transistors in the inverter. Besides, the vector control algorithms based on specially-designed d, q-axis current injection are needed to generate the control signals. Moreover, a programmatic virtual switch is used to select the working mode of the system. Without emergency, port s_2 is connected and the PMSM drive is controlled by the double closed-loop regulation strategy [31], [32]. During the normal operations, the reference speed ω_{ref} of the motor might be set to different levels for the sake of speed regulation, ranging from zero to the maximum attainable value. Once an emergency occurs, port s_1 is connected and the hybrid discharge algorithm is executed. This part will give a design method for the BR, and on this ground the bleeder size and weight reductions are analyzed. Then, different discharge regulation modes and algorithms are developed considering the initial condition when an active discharge is requested.

A. Design of BR for Proposed Discharge Method

When designing the hybrid discharge system, the extreme condition at which the initial speed ω_{m0} equals the maximum value needs to be considered. For the sake of simplicity, the vehicle powertrains that do not use flux-weakening control strategies for speed regulation are investigated in this paper, so the maximum machine speed can be assumed to equal the rated value ω_{rated}. In this case, the total energy to be dissipated is denoted as Q_{b_des}, which can be calculated by (13).

a) Resistance of BR

By contrast with the individual bleeder-based discharge method of which braking torque is produced depending on the quotient of the bus voltage and BR, as is shown in (7). The deceleration process of the new approach relies on the injected d, q-axis currents (transformed from the phase currents i_a and i_c). Further, another crucial feature of the proposed hybrid discharge technique is that, thanks to the BR, it is not necessary to adopt the piecewise q-axis reference current to avoid the voltage surge phenomenon as long as the resistance is relatively small. The reason is as follows: the voltage surge arises because within a short period, the rotor kinetic energy that is converted into the electric energy (KETEE) is larger than the total bleeding capacity (sum of internal and external dissipation). However, for the hybrid method, once the bus voltage rises

TABLE III
PROPERTIES OF BLEEDING RESISTOR

Resistor properties	Value	Unit
resistance R_b	18.8	Ω
current level i_{b_exRMS}	8.18	A
minimum diameter d_b	2.4	mm
required length l_b	173.5	m
calculated mass m_b	6.98	kg

greatly, the instantaneous bleeding power of the BR will shoot up and the short-period bleeding energy would surpass the KETEE, preventing the capacitor voltage from continuous growth. Based on these, a constant large q-axis reference current that can ensure the five-second discharge requirement is needed. According to (7) and (8), the q-axis current for design ($i_{qref\text{-}des}$) within t_r should track the following locus:

$$i_{qref\_des} = \frac{J(\omega_{th} - \omega_{rated})}{1.5pt_r\Psi_f} \tag{16}$$

where i_{dref_des} is the negative d-axis current for design.

Although the q-axis current in the machine is inclined to remain at the reference level when bleeding enters into the stable state, at the beginning instant of discharge, the real value of the q-axis current can still be influenced by the quotient of the initial capacitor voltage and BR because the DC component of the bus current i_{dc} (active current, directly related to i_q) in Fig.3 is approximately equal to i_b. In order to rapidly compel the q-axis current to trace the targeting value, we let the resistance of the BR satisfy:

$$R_b = \frac{U_{dc0}}{|i_{qref\_des}|} \tag{17}$$

b) Conductor design considering BR size and weight

Assume that during discharge, the energy dissipated by the external bleeder is Q_{bex_des} while Q_{bin_des} is the energy consumed by the machine windings, where $Q_{bex\_des} + Q_{bin\_des} = Q_{b\_des}$. Then, the RMS discharge current i_{b_exRMS} of the BR is:

$$i_{b\_exRMS} = \sqrt{\frac{Q_{bex\_des}}{R_b t_r}} \tag{18}$$

i_{b_exRMS} is vital to the conductor diameter and length of the BR whose resistance has been decided. Hence, in order to reduce the size and weight of the bleeder circuits as much as possible, i_{b_exRMS} should be minimal. Consequently, when designing the BR, Q_{bex_des} is supposed to be the lowest in the extreme condition. In this case, the best bleeding capacity of the machine windings needs to be utilized. Based on this, the currents in the machine is expected to be controlled to maintain at the system safe current (SSC) I_{max}, which should not pose any potential risks (including thermal damage and overcurrent, etc.) to the system during the whole discharge process, that is,

$$i_{dref\_des}^{\ 2} + i_{qref\_des}^{\ 2} = I_{max}^{\ 2} \tag{19}$$

Then, Q_{bex_des} is calculated by:

$$Q_{bex\_des} = Q_{b\_des} - I_{max}^{\ 2} R_s t_r \tag{20}$$

Substitute (16)-(18) and (20) into (15), the required diameter of the BR conductor is:

$$d_b = -3.765 + \sqrt{14.615 + 2.843\sqrt{\frac{J(Q_{b\_des} - I_{max}^{\ 2} R_s t_r)(\omega_{rated} - \omega_{th})}{1.5pt_r^{\ 2}\Psi_f U_{dc0}}}} \tag{21}$$

And the length is:

$$l_b = \frac{\pi R_b d_b^{\ 2}}{4\rho_r} \cdot 10^{-6} \tag{22}$$

The mass of the required conductor can be calculated by:

$$m_b = \frac{\pi}{4}\rho_m d_b^{\ 2} l_b \cdot 10^{-6} \tag{23}$$

c) Evaluation of size and weight reduction

Concerning the PMSM drive system whose parameters are in Table I, the properties of the designed BR are shown in Table III. In comparison with Table II, the required BR resistance in the proposed system increases to 18.8 Ω, but the conductor diameter d_b decreases to 2.4 mm (46.7%) and the length l_b drops to 173.5 m (27%). Importantly, the weight of the BR conductor experiences a significant decline from 33.6 to 6.98 kg.

Overall, the BR in the hybrid discharge structure are much smaller than that in the bleeder-based discharge system.

B. Discharge Modes and Control Algorithms

After adopting the above-mentioned hybrid bus voltage discharge topology, the EV powertrain is endowed with the ability to regulate the bus voltage to drop below the safe level within five seconds when the emergency happens at the speed of rated position. However, it is probable that the active discharge is requested at the moment when the machine does not reach the highest speed, including the standstill state. Considering the safety of the EV powertrain, especially the fragile transistors in the inverter, it is unnecessary to always control the d, q-aixs discharge currents to remain at the extreme states (i_{dref_des} and i_{qref_des}), and even the winding-based discharge part can be absent. Three types of discharge modes based on ω_{m0} and the corresponding control algorithms are developed in this section (as in Fig.5).

a) Full-power discharge mode

When an active discharge is requested at the speed of the maximum value, both the internal machine windings and the external bleeder circuits are needed for dissipating the residual energy. In this case, the hybrid system has to take full advantage of its own discharge capacity and the required discharge current I_r equals I_{max}. Consequently, the d, q-axis discharge currents (i_{d_dis} and i_{q_dis}) in the machine should comply with the calculated parameters during BR design:

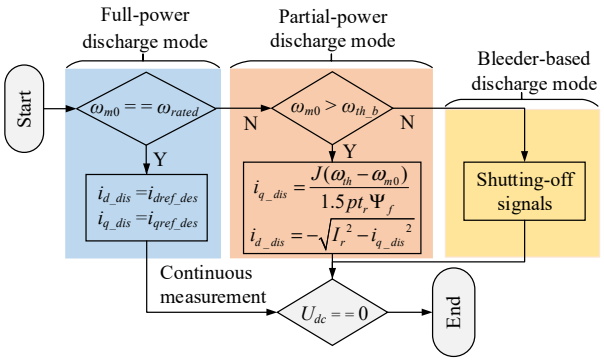

Fig. 5. Discharge modes and control algorithms.

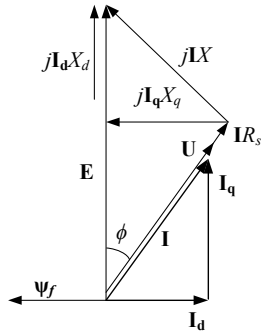

Fig. 6. Approximated PMSM phasor diagram operating as a generator.

$$\begin{cases} i_{q\_dis} = i_{qref\_des} \\ i_{d\_dis} = -\sqrt{I_{\max}{}^2 - i_{q\_dis}} \end{cases} \tag{24}$$

It is expected that the DC-bus capacitor voltage will get down to U_{safe} soon by the use of the combined scheme, removing the electrical shock risks. After that, the controller will continue to implement the discharge algorithms until the bus voltage arrives at zero.

b) Partial-power discharge mode

When ω_{m0} is lower than ω_{rated} but higher than the corner threshold ω_{th_b} below which only the external BR is able to pull the bus voltage down to 60 V within 5 s, both the windings and BR have to be adopted for discharge as well, but other than (24), the d, q-aixs current in the machine can be modest.

Firstly, the fast discharge requirement must be satisfied, so the q-axis discharge current should be controlled as:

$$i_{q\_dis} = \frac{J(\omega_{th} - \omega_{m0})}{1.5p\Psi_f t_r} \tag{25}$$

Secondly, as is illustrated in Fig.4, the bleeder circuits together with the bus capacitor constitute the load of the PMSM that works as a generator. Since the capacitance is usually small, the load can be further approximated as a resistor [27], [33]. Then, ignoring the mutual inductance, the current and voltage in a permanent magnet generator can be depicted by an approximated phasor diagram in Fig.6, X_d and X_q are the d and q-axis reactance; X=X_d+X_q, representing the machine reactance. $\mathbf{I}_d$ and $\mathbf{I}_q$ are the d and q-axis current vector; $\mathbf{U}$ is the phase voltage, and $\mathbf{I}$ is the current (amplitude is I) in the machine. Then, we can obtain that:

$$U_{dc} = \sqrt{3}(E\cos\phi - IR_s) = \sqrt{3}\left(\frac{C_e'\Psi_f\omega_m i_{q\_dis} - I^2R_s}{I}\right) \tag{26}$$

Between 0 and t_r, the energy dissipated by windings (Q_{bin}) and BR (Q_{bex}) can be represented as:

$$\begin{cases} Q_{bin} = \int_0^{t_r} 3I^2R_s\mathrm{d}t = 3I^2R_st_r \\ Q_{bex} = \int_0^{t_r} \frac{U_{dc}{}^2}{R_b}\mathrm{d}t \end{cases} \tag{27}$$

where Q_{bex} + Q_{bin} =Q_b. According to (7), (8) and (25)-(27), when $\omega_{m0} \le \omega_{rated}$, the required discharge current I_r in the machine will satisfy the following condition:

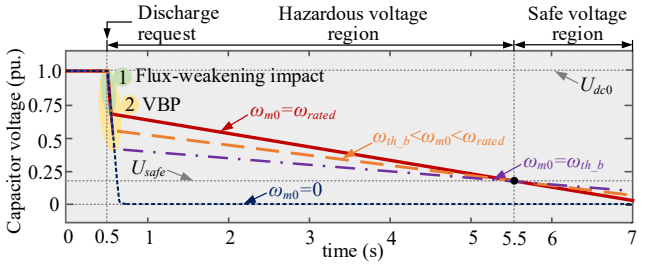

Fig. 7. Theoretical DC-bus capacitor voltage discharge characteristics under different control modes.

$$I_r^2 = \frac{3t_rR_s(ct_r + 2g) + Q_bR_b + \sqrt{Q_b^2R_b^2 - c^2t_r^4R_s(12R_b - 3R_s) + 6R_bR_st_r[(6gt_r - Q_b)(ct_r - g) + Q_bg]}}{3R_st_r(R_b + R_s)} \tag{28}$$

where c=$\frac{1.5pC_e'\Psi_f{}^2 i_{q\_dis}{}^2}{J}$ and g=$C_e'\Psi_f\omega_{m0}i_{q\_dis}$. Therefore, the d-axis reference discharge current should be set as:

$$i_{d\_dis} = -\sqrt{I_r^2 - i_{q\_dis}{}^2} \tag{29}$$

Similar to the full-power discharge mode, only when the bus voltage gets down to zero will the implementation stops.

c) Bleeder-based discharge mode

There must be a speed threshold ω_{th_b} below which (including standstill case) there is no need to implement the winding-based discharge algorithms and just the bleeder-based strategy is qualified for the five-second discharge process.

According to (5) and (6), the bus voltage generated by ω_{m0} is:

$$U_{dc}(0) = \frac{\sqrt{3}C_e'\Psi_fR_b\omega_{m0}}{R_b + 2R_s} \tag{30}$$

Obviously, $U_{dc}(0)$ is smaller than U_{dc0} when the initial speed is less than ω_{rated}. But since we have evaluated that the resistance of BR is small, the capacitor voltage will quickly decline to the back EMF level, which is called voltage balance phenomenon (VBP, eg., balance time<20 ms for the aforementioned system). Then, the DC-bus capacitor voltage will be dominated by the induced voltage. On this ground the differential equation (10) can be solved with the boundary condition $U_{dc}(0)$ after ignoring the balance time.

$$U_{dc}(t) = U_{dc}(0)\cdot\exp\left(-\frac{1.5\sqrt{3}C_e'p\Psi_f{}^2}{J(R_b + 2R_s)}t\right) \tag{31}$$

when t=t_r, U_{dc} should be less than U_{safe}. So it can be derived that:

$$\omega_{th\_b} = \frac{U_{safe}(R_b + 2R_s)}{\sqrt{3}C_e'\Psi_fR_b\exp\left(-\frac{1.5\sqrt{3}C_e'p\Psi_f{}^2}{J(R_b + 2R_s)}t_r\right)} \tag{32}$$

When ω_{m0} < ω_{th_b}, the "shutting-off" signals will be directly applied to the inverter.

Fig.7 demonstrates the theoretical bus voltage characteristics under the three different discharge modes. Three main features can be summarized as follows:1) When the machine windings serve for discharge, apart from ω_{m0}, the negative injected flux-weakening current (d-axis current) is another key factor that makes the back EMF of the machine lower than U_{dc0}, resulting in VBP. Therefore, the bus voltage will experience a

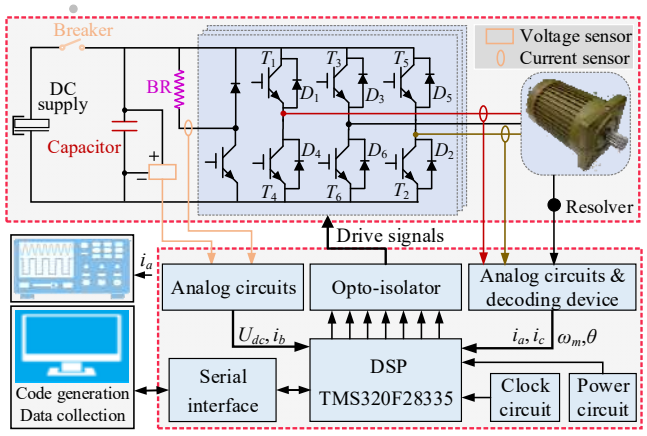

(a)

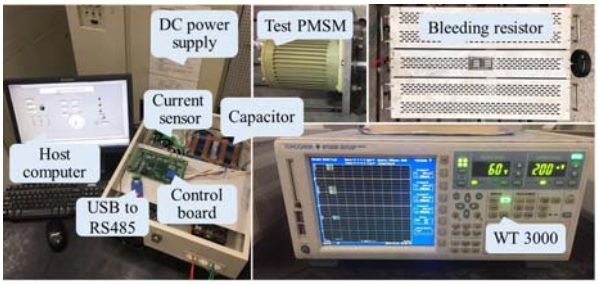

(b)

Fig. 8. Test bench. (a) Circuit diagram. (b) Experimental equipment.

sharp decrease immediately after the discharge request arises even when the initial speed equals ω_{rated}. 2) When the capacitor voltage is determined by the machine (ω_{m0}>0), the higher the initial speed is, the larger the VDR becomes at the same discharge moment. 3) In theory, the bus voltage will quickly drop to zero for both the full-power and partial power discharge modes in the safe voltage region. But it lasts long for the bleeder-based discharge mode, which is allowable in this research because the voltage shock risks have been eliminated.

IV. EXPERIMENTAL VERIFICATIONS

Experiments are conducted on a three-phase SPMSM whose parameters are consistent with Table I. The experimental circuit diagram and equipment are shown in Fig.8 (a) and (b), respectively. The winding resistance can be regulated by directly connecting steel wire with high resistivity for research. A DC power supply is available at 312 V. An intelligent power module (IPM), Mitsubishi PM100RLA120, is used as the voltage source inverter with the frequency of 7.5 kHz. Four thin-film capacitors, DHF DAWNCAP 140 μF, are connected in parallel to compose the 560 μF DC-bus capacitor. In order to verify the effectiveness of the designed BR resistance, a slide rheochord of which resistance can be adjusted to 18.8 Ω (current level 15 A) function as the BR. The proposed discharge modes and control algorithms are implemented on a DSP TMS320F28335 controller board. Hall current sensors (HNC-100LT) that are connected to WT3000 are used to measure the machine phase currents during test, while the motor *d*, *q*-axis and BR currents are calculated and recorded by

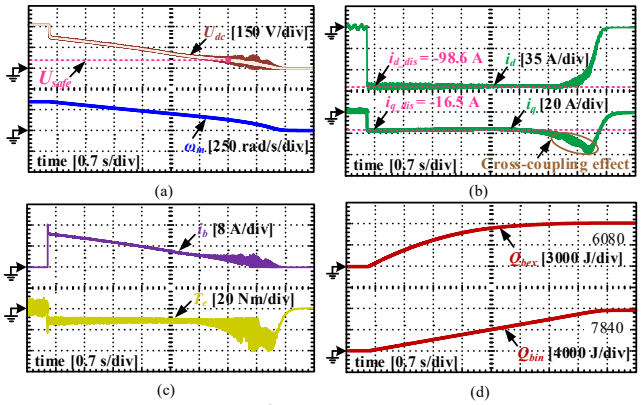

Fig. 9. Experimental results of the proposed discharge method when emergency occurs at the speed of 345 rad/s. (a) DC-bus voltage and machine speed. (b) Discharge *d*, *q*-axis currents. (c) BR current and braking torque. (d) Energy dissipated by BR and machine windings.

the digital controller. The DC-bus voltage is measured by a voltage transducer LV25-P.

Firstly, assume an active discharge request occurs when the motor speed is ω_{rated}. At this moment, the system operates at the full-power discharge mode, and the reference *d* and *q*-axis reference currents can be calculated as -98.6 A and -16.5 A, respectively. Overall, Fig.9 (a) illustrates that the capacitor voltage drops to the safe level within around 4.4 s, being slightly shorter than 5 s. This happens because the mechanical friction is ignored when establishing the discharge model. It can be concluded that the proposed BR design and full-power discharge methods are very effective. In terms of the speed characteristics, interestingly, the machine speed is still higher than ω_{th} when the DC bus voltage arrives at 60 V, which is caused by the flux-weakening impact. This also contributes to shortening the discharge time. In accordance with the theoretical analysis, the bus voltage experiences sharp decrease (VBP) after the discharge algorithms are implemented. In Fig.9 (b), both the *d* and *q*-axis currents get to the expected level quickly after discharge begins and then, they level off until about 4.9 s when the bus voltage is not able to maintain such high current level. Due to the cross-coupling effect [34], the magnitude of the *q*-axis current experiences a short-period increase before it declines to zero, while the *d*-axis current continuously decreases because of its large value. Fig.9 (c) shows that the bleeding current passing through the BR (BR current) jumps to about 16 A at first. This phenomenon is caused by the initial voltage of the capacitor. Then, the discharge BR current will be dominated by the back EMF, witnessing a linearly downward trend. Moreover, the braking torque is consistent with the *q*-axis current, indicating that the torque calculation method is reasonable. Finally, at the extreme state, a total of 13920 J (6080 and 7840 J for external BR and internal windings, respectively) are dissipated by the whole system.

Fig. 10 and Fig.11 depict the experimental results when the emergency occurs at the speed of 250 rad/s and 200 rad/s, respectively. In these cases, the partial-discharge mode is employed. In Fig.10, the *d*, *q*-axis discharge currents require to be set as -54.5 and -11 A, respectively. The capacitor voltage

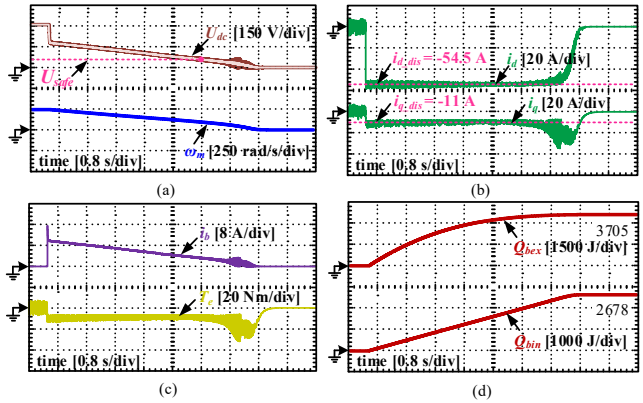

Fig. 10. Experimental results of the proposed discharge method when emergency occurs at the speed of 250 rad/s. (a) DC-bus voltage and machine speed. (b) Discharge *d*, *q*-axis currents. (c) BR current and braking torque. (d) Energy dissipated by BR and machine windings.

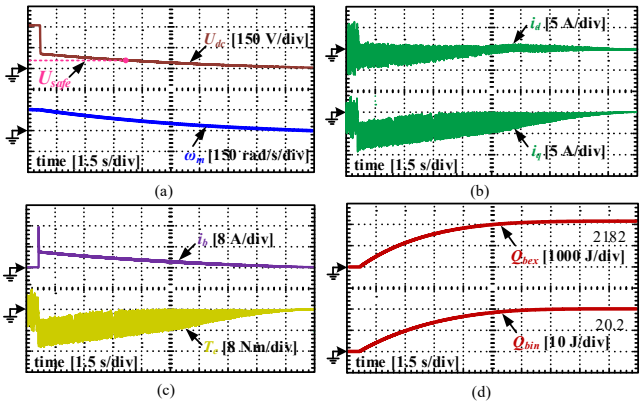

Fig. 12. Experimental results of the proposed discharge mode when emergency occurs at the speed of 150 rad/s. (a) DC-bus voltage and machine speed. (b) Discharge *d*, *q*-axis currents. (c) BR current and braking torque. (d) Energy dissipated by BR and machine windings.

gets down to the safe level at about 4.8 s (discharge period is 4.3 s). Similar to the extreme state, when the bus voltage is 60 V, the rotating speed is about 98 rad/s which is higher than the threshold. As for the discharge currents, both the *d* and *q*-axis currents can track the reference values well as long as the bus voltage is high enough. The BR current in Fig.10 (c) witnesses a sudden increase at the start of discharge (16 A as well) before it enters into the linear declining region. Fig.10 (d) illustrates that about 3705 J energy is consumed by bleeder circuits while 2678 J is dissipated by the machine windings in the format of heat. The VDR in Fig.11 (a) gets smaller than that in Fig.10 (a) because the initial speed has gotten lower but the discharge period sees little change. When the initial speed is 200 rad/s, the *d*, *q*-axis discharge currents are -42 and -8 A, respectively. Obviously, the braking torque in Fig.11 (c) is smaller than that in Fig.10 (c), indicating that the discharge process becomes more modest.

Fig.12 demonstrates the experimental results when the discharge request arises at the speed of ω_{th_b}. Under the bleeder-based discharge method, there are no specially designed currents that are injected into the machine. The induced voltage will generate bleeding current through the UR. Fig.12 (a) shows that it is nearly 4.1 s before the bus voltage arrives at the safe level, but the total discharge time is over 10 s.

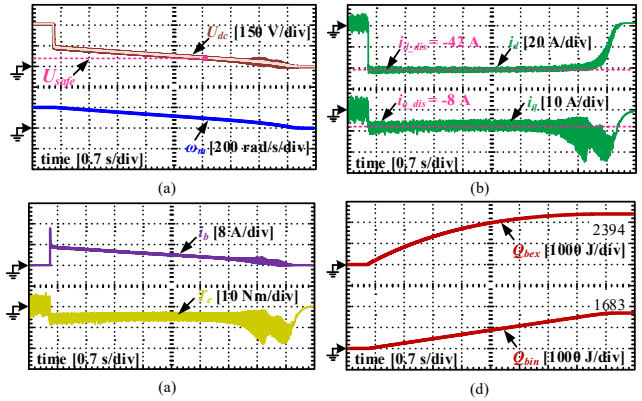

Fig. 11. Experimental results of the proposed discharge method when emergency occurs at the speed of 200 rad/s. (a) DC-bus voltage and machine speed. (b) Discharge *d*, *q*-axis currents. (c) BR current and braking torque. (d) Energy dissipated by BR and machine windings.

This happens because the braking torque which is related to the bleeding current remains declining (as in Fig.12 (c)), leading to the speed deceleration gets lower. Fig.12 (b) presents that the *d*-axis component is much smaller than the *q*-axis component of the current in the machine, indicating that the assumption for equation (7) is reasonable. Finally, Fig12. (d) shows that most residual energy (2182 J) is dissipated by the BR and only 20.2 J is consumed by the machine windings. Before leaving Fig.12, an interesting phenomenon that the output electromagnetic torque of the machine fluctuates greatly during the discharge process should not be ignored. This happens due to the following reasons. It needs to be mentioned that the torque is directly observed by (7), so the dynamics of the torque see the similar trend with the *q*-axis current. Notably, the torque experiences a step change immediately when an active discharge is requested. Meanwhile, when the *q*-axis current declines as the bus voltage decreases, the magnitude of the torque will gradually drop as well. Further, because the PMSM works as a three-phase generator and the inverter functions as an UR (as in Chapter II) when the bleeder-based discharge mode is activated, the currents in each phase of the machine are not continuous (with fluctuations) due to the properties of an UR [35]. Even worse, there exist the moments at which only two-phase windings are conducted and the other phase is shut off in each electrical period. Consequently, when transforming

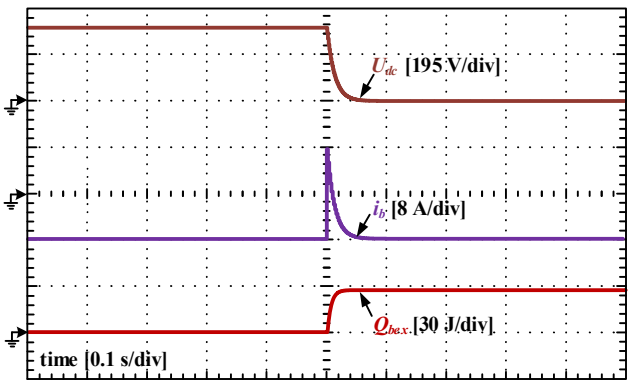

Fig. 13. Experimental results of the proposed discharge mode when emergency occurs at the speed of zero.

the three-phase currents into the ones in the rotating reference frame, large fluctuations will be witnessed as in Fig.12 (b). Further, the output braking torque will be influenced so as to be fluctuant as in Fig.12 (c).

Given that the discharge is requested when the machine speed is zero, the experimental results are shown in Fig.13. The bus voltage can drop to zero within about 0.03 s, which means the voltage balance time is really short and the safety can be ensured. All of the energy stored in the capacitor (about 27 J) will be consumed by the BR.

Overall, according to the experimental results, the proposed full-power discharge algorithm, the partial-power discharge algorithm and the bleeder-based discharge algorithm are proven to be able to achieve fast discharge within five seconds for the tested system, complying with the requirements in the United Nation Vehicle Regulation ECE R94.

V. CONCLUSION

This paper proposes a novel combined residual energy discharge strategy based on the internal windings and the external bleeder circuits to achieve the fast discharge requirement without greatly sacrificing the BR size and weight for PMSM based EV powertrains in emergency.

1) An accurate model for the traditional external bleeder-based discharge method is established to explicitly evaluate the BR size and weight sacrifice, explaining that it is necessary to develop the superior hybrid discharge technique.

2) The combined discharge strategy that synthesizes the advantages of the traditional winding-based and bleeder-based discharge schemes is detailedly illustrated. Firstly, the external BR resistance is designed based on the extreme working condition, and the advantages over the traditional bleeder-based discharge approach are analyzed. Then, according to the different machine states at the moment of emergency occurrence, three different discharge modes (full-power, partial-power and bleeder-based modes) and the corresponding control algorithms are given.

The experiments are carried out on a PMSM used for EVs, verifying that the novel discharge technique is effective. Consequently, the proposed BR parameter design method and the different control modes can be applied in the real cases.

REFERENCES

[1] H. Liu, Z. Q. Zhu, E. Mohamed, Y. Fu and X. Qi, "Flux-Weakening Control of Nonsalient Pole PMSM Having Large Winding Inductance, Accounting for Resistive Voltage Drop and Inverter Nonlinearities," in *IEEE Transactions on Power Electronics*, vol. 27, no. 2, pp. 942-952, Feb. 2012.

[2] J. Lu, X. Zhang, Y. Hu, J. Liu, C. Gan and Z. Wang, "Independent Phase Current Reconstruction Strategy for IPMSM Sensorless Control Without Using Null Switching States," in *IEEE Transactions on Industrial Electronics*, vol. 65, no. 6, pp. 4492-4502, June 2018.

[3] G. Wang, L. Yang, G. Zhang, X. Zhang and D. Xu, "Comparative Investigation of Pseudorandom High-Frequency Signal Injection Schemes for Sensorless IPMSM Drives," in *IEEE Transactions on Power Electronics*, vol. 32, no. 3, pp. 2123-2132, March 2017.

[4] K. Baoquan, L. Chunyan and C. Shukang, "Flux-Weakening-Characteristic Analysis of a New Permanent-Magnet Synchronous Motor Used for Electric Vehicles," in *IEEE Transactions on Plasma Science*, vol. 39, no. 1, pp. 511-515, Jan. 2011.

[5] C. Ma and S. Zuo, "Black-Box Method of Identification and Diagnosis of Abnormal Noise Sources of Permanent Magnet Synchronous Machines for Electric Vehicles," in *IEEE Transactions on Industrial Electronics*, vol. 61, no. 10, pp. 5538-5549, Oct. 2014.

[6] G. Feng, C. Lai, K. L. V. Iyer and N. C. Kar, "Improved High-Frequency Voltage Injection Based Permanent Magnet Temperature Estimation for PMSM Condition Monitoring for EV Applications," in *IEEE Transactions on Vehicular Technology*, vol. 67, no. 1, pp. 216-225, Jan. 2018.

[7] T. Wang, C. Liu, G. Lei, Y. Guo and J. Zhu, "Model predictive direct torque control of permanent magnet synchronous motors with extended set of voltage space vectors," in *IET Electric Power Applications*, vol. 11, no. 8, pp. 1376-1382, Sep. 2017.

[8] X. Liu, D. Wu, Z. Q. Zhu, A. Pride, R. P. Deodhar and T. Sasaki, "Efficiency Improvement of Switched Flux PM Memory Machine Over Interior PM Machine for EV/HEV Applications," in *IEEE Transactions on Magnetics*, vol. 50, no. 11, pp. 1-4, Nov. 2014, Art no. 8202104.

[9] Y. Miyama, M. Hazeyama, S. Hanioka, N. Watanabe, A. Daikoku and M. Inoue, "PWM Carrier Harmonic Iron Loss Reduction Technique of Permanent-Magnet Motors for Electric Vehicles," in *IEEE Transactions on Industry Applications*, vol. 52, no. 4, pp. 2865-2871, July-Aug. 2016.

[10] L. Dang, N. Bernard, N. Bracikowski and G. Berthiau, "Design Optimization with Flux Weakening of High-Speed PMSM for Electrical Vehicle Considering the Driving Cycle," in *IEEE Transactions on Industrial Electronics*, vol. 64, no. 12, pp. 9834-9843, Dec. 2017.

[11] C. Gong, Y. Hu, G. Chen, H. Wen, Z. Wang and K. Ni, "A DC-Bus Capacitor Discharge Strategy for PMSM Drive System With Large Inertia and Small System Safe Current in EVs," in *IEEE Transactions on Industrial Informatics*, vol. 15, no. 8, pp. 4709-4718, Aug. 2019.

[12] S. Ashida, K. Yamada, M. Nakamura, T. Shimana, and T. Soma, "Electric vehicle, and control apparatus and control method for electric vehicle," U.S.Patent 8631894 B2, Jan. 21, 2014.

[13] Z. Ke, J. Zhang and M. W. Degner, "DC Bus Capacitor Discharge of Permanent-Magnet Synchronous Machine Drive Systems for Hybrid Electric Vehicles," in *IEEE Transactions on Industry Applications*, vol. 53, no. 2, pp. 1399-1405, March-April 2017.

[14] United Nation Economic Commission for Europe Vehicle Regulation, No.94 (ECE R94), Unifrom provisions concerning the approval of vehicles with regard to the protection of the occupants in the event of a frontal collision, Rev. 2, Annex 11, Aug. 2013.

[15] K. Itani, A. De Bernardinis, Z. Khatir, A. Jammal and M. Oueidat, "Regenerative Braking Modeling, Control, and Simulation of a Hybrid Energy Storage System for an Electric Vehicle in Extreme Conditions," in *IEEE Transactions on Transportation Electrification*, vol. 2, no. 4, pp. 465-479, Dec. 2016.

[16] Y. Li, J. Zhang, C. Lv, D. Kong and C. He, "Research of Regenerative Braking System for Electrified Buses Equipped with a Brake Resistor," *2013 IEEE Vehicle Power and Propulsion Conference (VPPC)*, Beijing, 2013, pp. 1-5.

[17] H. Peng, J. Wang, W. Shen, D. Shi and Y. Huang, "Controllable regenerative braking process for hybrid battery–ultracapacitor electric drive systems," in *IET Power Electronics*, vol. 11, no. 15, pp. 2507-2514, Dec. 2018.

[18] R. Phukan, J. Hu, J. Ulrich and L. Wei, "Bus Conditioner and Discharge Circuit in Floating Ground System Applications," *2018 IEEE Energy Conversion Congress and Exposition (ECCE)*, Portland, OR, 2018, pp. 1816-1821.

[19] T. Goldammer, T. Le, J. Miller, and J. Wai, "Active high voltage bus bleed down," U.S. Patent 20120161679 A1, Jun. 28, 2012.

[20] Z. Ke, J. Zhang and M. W. Degner, "DC bus capacitor discharge of permanent magnet synchronous machine drive systems for hybrid electric vehicles," *2016 IEEE Applied Power Electronics Conference and Exposition (APEC)*, Long Beach, CA, 2016, pp. 241-246

[21] C. Gong, Y. Hu, H. Wen, G. Chen, W. Li and J. Gao, "Reliable Winding-based DC-Bus Capacitor Discharge Technique Over Full-Speed Range for IPMSM Drive in Electric Vehicles Without Position Sensor," in *IEEE Transactions on Industrial Electronics*. doi: 10.1109/TIE.2019.2946550.

[22] J. Pan *et al*., "A Novel Discharging Control Strategy for Modular Multilevel Converter Submodules without Using External Circuit," *2018 IEEE Energy Conversion Congress and Exposition (ECCE)*, Portland, OR, 2018, pp. 656-661.

[23] J. Pan *et al*., "Zero-Cost Closed-Loop Discharging Method for Modular Multilevel Converter Submodules Without External Circuits," in *IEEE Transactions on Industry Applications*, vol. 55, no. 5, pp. 4846-4854, Sept.-Oct. 2019.

[24] J. Lara, J. Xu and A. Chandra, “Effects of Rotor Position Error in the Performance of Field-Oriented-Controlled PMSM Drives for Electric Vehicle Traction Applications,” in *IEEE Transactions on Industrial Electronics*, vol. 63, no. 8, pp. 4738-4751, Aug. 2016.
[25] A. Athavale, K. Sasaki, B. S. Gagas, T. Kato and R. D. Lorenz, "Variable Flux Permanent Magnet Synchronous Machine (VF-PMSM) Design Methodologies to Meet Electric Vehicle Traction Requirements with Reduced Losses," in *IEEE Transactions on Industry Applications*, vol. 53, no. 5, pp. 4318-4326, Sept.-Oct. 2017.
[26] V. Ruuskanen, J. Nerg, M. Rilla and J. Pyrhönen, “Iron Loss Analysis of the Permanent-Magnet Synchronous Machine Based on Finite-Element Analysis Over the Electrical Vehicle Drive Cycle,” in *IEEE Transactions on Industrial Electronics*, vol. 63, no. 7, pp. 4129-4136, July 2016.
[27] Chong-Zhi Liaw, W. L. Soong, B. A. Welchko and N. Ertugrul, “Uncontrolled generation in interior permanent-magnet Machines,” in *IEEE Transactions on Industry Applications*, vol. 41, no. 4, pp. 945-954, July-Aug. 2005.
[28] J. Liu, C. Gong, Z. Han and H. Yu, “IPMSM Model Predictive Control in Flux-Weakening Operation Using an Improved Algorithm,” in *IEEE Transactions on Industrial Electronics*, vol. 65, no. 12, pp. 9378-9387, Dec. 2018.
[29] X. Zhang, L. Zhang and Y. Zhang, “Model Predictive Current Control for PMSM Drives With Parameter Robustness Improvement,” in *IEEE Transactions on Power Electronics*, vol. 34, no. 2, pp. 1645-1657, Feb. 2019.
[30] S. Xiaoxia, W. Yichun, Meng Lingke, Wang Facheng and Xiang Longyun, “Research on braking resistor of hybrid electric armored vehicle,” *2010 International Conference on Information, Networking and Automation (ICINA)*, Kunming, 2010, pp. V2-206-V2-210.
[31] Z. Zhang, R. Ma, L. Wang and J. Zhang, “Novel PMSM Control for Anti-Lock Braking Considering Transmission Properties of the Electric Vehicle,” in *IEEE Transactions on Vehicular Technology*, vol. 67, no. 11, pp. 10378-10386, Nov. 2018.
[32] G. Feng, C. Lai and N. C. Kar, “A Closed-Loop Fuzzy-Logic-Based Current Controller for PMSM Torque Ripple Minimization Using the Magnitude of Speed Harmonic as the Feedback Control Signal,” in *IEEE Transactions on Industrial Electronics*, vol. 64, no. 4, pp. 2642-2653, April 2017.
[33] C. Gong, Y. Hu, C. Gan, G. Chen and A. Mohammed, “Modelling, Analysis and Attenuation of Uncontrolled Generation for IPMSM based Electric Vehicles in Emergency,” in *IEEE Transactions on Industrial Electronics*. doi: 10.1109/TIE.2019.2926049
[34] A. Rabiei, T. Thiringer, M. Alatalo and E. A. Grunditz, “Improved Maximum-Torque-Per-Ampere Algorithm Accounting for Core Saturation, Cross-Coupling Effect, and Temperature for a PMSM Intended for Vehicular Applications,” in *IEEE Transactions on Transportation Electrification*, vol. 2, no. 2, pp. 150-159, June 2016.
[35] Z. Zhang, X. Zou, Z. Wu and Y. Zou, "Analysis on Harmonic Current of Three-phase Bridge Uncontrolled Rectifier," *2010 Asia-Pacific Power and Energy Engineering Conference*, Chengdu, 2010, pp. 1-4.

Chao Gong (S’19) was born in Shandong province in P.R. China, on February 22, 1991. He received the B.Eng. and the M.Eng degree in electrical engineering from Northwestern Polytechnical University, Xi’an, China, in 2014 and 2016, respectively. Currently, he is a PHD student with the major of Electrical Engineering in the Department of Electronic Engineering of University of York, Heslington, York, the UK.

His research interests include electrical machine design and drives and motion control.

Yihua Hu (M’13-SM’15) received the B.S. degree in electrical motor drives in 2003, and the Ph.D. degree in power electronics and drives from China University of Mining and Technology, in 2003 and 2011, respectively.

Between 2011 and 2013, he was with the College of Electrical Engineering, Zhejiang University as a Postdoctoral Fellow. Between 2013 and 2015, he worked as a Research Associate at the power electronics and motor drive group, the University of Strathclyde. Currently, he is a Reader at the Department of Electronic Engineering, University of York (UoY). His research interests include renewable generation, power electronics converters & control, electric vehicle, more electric ship/aircraft, smart energy system and non-destructive test technology. He is the associate editor of IET Renewable Power Generation, IET Intelligent Transport Systems and Power Electronics and Drives.

Wenzhen Li was born in Xinjiang province in P.R. China, on April 22, 1991. She received the B.Eng. degree in electrical engineering from Henan University of Technology, Zhengzhou, China, in 2012, and the M.Eng degree in control engineering from Xi`an Polytechnic University, Xi’an, China, in 2015. She is currently working toward the Ph.D. degree with the major of electrical engineering at the Northwestern Polytechnical University, Xi’an, China.

Her research interests include permanent magnet synchronous motor drives and sensorless control.

Jinqiu Gao was born in Shannxi province in P.R. China, on January 07, 1996. She received the B.Eng. degree in electrical engineering from Northwestern Polytechnical University, Xi’an, China, in 2017. Currently, she is a Master student with the major of Electrical Engineering in the School of Automation, Northwestern Polytechnical University, Xi’an, China.

Her research interests include electrical machines design and drives and motion control.

Jinglin Liu (M’01) received the B.Eng. degree in electrical engineering from Tsinghua University, Beijing, China, in 1986, and the M.Eng. and the Ph.D. degrees in electrical engineering from Northwestern Polytechnical University, Xi’an, China, in 1990 and 2002, respectively. Since 1994, he has been a Faculty Member with Northwestern Polytechnical University, Xi’an, where he is currently a Professor of Electrical Engineering.

His research interests include electrical machines design and drives, power electronics, fault diagnosis, and motion control.

Huiqing Wen (M’13-SM’18) received his B.S. and M.S. degrees in Electrical Engineering from Zhejiang University, Hangzhou, China, in 2002 and 2006, respectively. In 2009, he received his Ph.D. in Electrical Engineering from the Chinese Academy of Sciences, Beijing, China. From 2009 to 2010, he has been an electrical engineer working with the GE (China) Research and Development Center Company, Ltd., Shanghai, China. From 2010 to 2011, he was an engineer at the China Coal Research Institute, Beijing, China. From 2011 to 2012, he was a postdoctoral fellow at the Masdar Institute of Science and Technology, Abu Dhabi, United Arab Emirates. In 2013, he joined the Electrical and Electronic Engineering Department of Xi’an Jiaotong-Liverpool University (XJTLU), Suzhou, China. Currently, he is a senior associate professor at the XJTLU. He has published more than 100 peer reviewed technical papers in leading journals/conferences and holds over 20 issued/pending patents. His research interests include renewable energy, electric vehicle, power electronics, Microgrid, and power semiconductor devices. He is the associate editor of IEEE ACCESS, International Journal of Photoenergy, and Journal of Power Electronics.

Jiankang Yang was born in Guizhou province in P.R. China, on December 01, 1995. He received the B.Eng. degree in electrical engineering from Wuhan University of Technology, Wuhan, China, in 2017. Currently, he is a Master student with the major of Electrical Engineering in the School of Automation, Northwestern Polytechnical University, Xi’an, China.

His research interests include electrical machines design.